Li2TiO3/Ni foam composite as high-performance electrode for energy storage and conversion

A. Lakshmi-Narayana, M. Dhananjaya, N. Guru-Prakash, A. Mauger, C.M.
Julien, O.M. Hussain

HAL Id: hal-02277631

https://hal.sorbonne-universite.fr/hal-02277631v1

Submitted on 3 Sep 2019

Li$_2$TiO$_3$/Ni foam composite as high-performance electrode for energy storage and conversion

A. Lakshmi-Narayana [a], M. Dhananjaya [a], N. Guru-Prakash [a], A. Mauger [b], C.M. Julien [b,*], O.M. Hussain [a]

[a] Thin Films Laboratory, Department of Physics, Sri Venkateswara University, Tirupati, 517502, India
[b] Sorbonne Université, UPMC Univ Paris 06, Institut de Minéralogie, de Physique des Matériaux et de Cosmochimie (IMPMC), CNRS UMR 7590, 4 place Jussieu, 75005 Paris, France

ARTICLE INFO

ABSTRACT

Li$_2$TiO$_3$/Ni foam composites were prepared by a solid-state reaction process. They crystallized in the monoclinic Li$_2$TiO$_3$ structure with $C2/c$ space group. SEM images show that the Li$_2$TiO$_3$ particles are monodispersed crystallites of average size 49 nm, infused into porous scaffold Ni foam. As an anode in lithium battery, the composite delivered a discharge capacity of 153 mAh g^{-1} in an aqueous electrolyte and retained 95% of its initial capacity after 30 cycles. Moreover, the Li$_2$TiO$_3$/Ni foam composite as a negative electrode of pseudo-supercapacitor delivered a specific capacitance of 593 F g^{-1} and retained 95% of its initial capacitance after 1000 cycles. The enhanced capacity of Li$_2$TiO$_3$/Ni composite is due to porous scaffold Ni foam, which provides high conductivity to the Li$_2$TiO$_3$ particles and high effective surface area for redox reactions. The performance of the Li$_2$TiO$_3$/Ni foam as an electrode material for both lithium-ion batteries (LIBs) and supercapacitors (SCs) shows that this composite is promising for energy storage devices.

1. Introduction

The issues of fossil energy consumption and environmental pollution have triggered a gold rush for exploitation of sustainable energy sources and effective conversion/storage techniques. Lithium-ion batteries (LIBs) and supercapacitors (SCs) with high-energy density and high-power density have appealed worldwide attention in meeting the mounting power demands of electronic devices [1, 2, 3]. However, materials often suffer from low conductivity, which affects the electrochemical properties. Therefore, there is a need to develop high performance electrode materials. The microstructure and surface morphology of electrode material make a great impact on the electrochemical performance [4]. Nanostructured transition-metal oxides (TMOs) such as TiO$_2$, Li$_4$Ti$_5$O$_{12}$, NiO, MnO$_2$, etc., with confined dimension effect and high surface area are advantageous to reduce electron and Li ions diffusion paths and increase active sites for Li insertion/extraction reaction in both LIBs and SCs. Among a wide variety of possible electrode materials based on TMOs, Li$_2$TiO$_3$ has focused attention because of its good structural performance and high theoretical capacity. In addition, it is cost effective and eco-friendly. Moreover, this material can be used either as an anode

for LIBs or an electrode for SCs [7] due to its three-dimensional path for Li$^+$ ion migration, with enhanced performance when the particles are nano-sized. In particular, one dimensional (1D) nanoparticles [5], nanofibers [6], nanowires [7], nanotubes [8], etc., display excellent electrochemical properties. The nanosize improves the cycling performance of electrodes since it facilitates the accommodation to the substantial volume changes throughout the cycling processes [9]. The drawback is the tendency of the nanostructured metal oxides to agglomerate [10]. One of the suitable solutions to overcome this problem is to grow the active materials directly on a Ni foam that has two advantages: it is conductive, and it insures a good mechanical strength.

As far as we know, there is no report on electrochemical properties of Li$_2$TiO$_3$/Ni foam composites. Hence, in the present study, nanocrystalline Li$_2$TiO$_3$ (denoted LTO) and Li$_2$TiO$_3$/Ni foam composites (denoted as LTO/Ni composite) were prepared by a simple solid-state reaction. The electrodes are characterized as anode materials for LIBs and potential electrodes for SCs, using cyclic voltammetry (CV), galvanostatic charge-discharge (CP) and cycling tests. This LTO/Ni composite demonstrated a high discharge capacity and high specific capacitance with good structural stability and improved cyclability.

---

* Corresponding author.
 E-mail address: christian.julien@upmc.fr (C.M. Julien).

2. Experimental

2.1. Synthesis procedure

Nanocrystalline Li_2TiO_3 sample was prepared by solid-state reaction. In this process, TiO_2 (anatase A.R) and Li_2CO_3 were used as source materials in a stoichiometric ratio (Li:Ti = 2:1). These raw materials were mixed with ethanol and ball-milled for 4 h at a speed of 400 rpm, with the ball feed ratio fixed at 5:1. The resultant mixture was transferred to a ceramic crucible and dried at 80 °C, followed by calcination at 800 °C for 5 h at a rate of 5 °C/min. The chemical reaction of this synthesis process has been described elsewhere [11]. The LTO powder thus obtained was ground for 3 h using agate mortar with the addition of N-methyl pyrrolidone (NMP). The resulting slurry was coated on nickel foam substrate (1 × 0.5 cm^2) and dried at 100 °C for 3 h to obtain the LTO/Ni composite. The Ni foam (Sigma Aldrich, USA) substrate had 110 pores per square inch. The pristine LTO was also investigated for comparison.

2.2. Sample characterization

The crystal structure of the LTO/Ni composite was analyzed by X-ray diffractometer (Siefert, model 3003 TT). The surface morphology was analyzed by a high-resolution transmission electron microscope (HRTEM-FEI microscope; TECHNAI G^2-30 S-twin D905) and field emission scanning electron microscope (FESEM) (Model SIRION 200). The recorded FESEM data were treated via the "Image NOVA" software (NTMDT) by generating the z-axis to develop a three-dimensional (3D) surface morphology picture and evaluate the surface roughness. The composition analysis of elements was carried out by energy dispersive spectroscopy (Model: Oxford instruments Inca Penta FETX3) attached with the SEM (model SEM ZEISS 40w).

2.3. Electrochemical tests

The electrochemical performances were analyzed using a 3-electrode aqueous-type cell. The cyclic voltammetry (CV) and chronopotentiometry (CP) experiments were conducted to determine the specific discharge capacity and specific capacitance. The specific capacity of the electrode was calculated excluding the electrochemically inert Ni foam mass, which acts as a current collector. The LTO/Ni composite working electrode was prepared by mixing the active material (LTO), carbon black (CB) and polyvinylidine fluoride (PVDF) in NMP with the ratio of 80:10:10 (in wt.%). After vigorous stirring, the resultant slurry was uniformly deposited on the Ni foam substrate (1 × 0.5 cm^2) and subsequently dried at 100 °C for 3 h in air. The mass loading was approximately 6 mg cm^{-2}. Platinum strip and Ag/AgCl were used as the counter and reference electrodes, respectively. A highly concentrated (3 mol L^{-1}) Li_2SO_4 aqueous solution was used as the electrolyte. The electrochemical workstation (Model: CHI608C) was employed to carry out the electrochemical analysis. The pristine LTO electrode was prepared following the same process as LTO/Ni composite. The experimental conditions are similar for pseudocapacitor tests but maintained at different current densities. It has been observed that the difference between peak current values (I_{pa} and I_{pc}) for battery property lies between ~ -3 to +6 mA g^{-1}, whereas pseudocapacitor has -0.36 to +0.57 mA g^{-1}. The variation in current densities and nanoscale particles are caused for dual nature in Li_2TiO_3/Ni foam composite. Because in actual aqueous conditions, Ni metal did not react with Li to form an Li-Ni alloys [12], Ni foam does not contribute any capacity to the composite, it serves as a conductive matrix to promote fast faradaic reactions to the Li_2TiO_3 particles. Moreover, the excellent electronic and ionic conductivity of the interconnected 3D-Ni architectures not only afford large surface area, high mechanical strength but also provide unblocked ion/electron pathway, which enables rapid ion/electron transport during the charge-discharge process.

3. Results and discussion

3.1. Structural and morphological properties

The structure and composition of the LTO/Ni composite was investigated by the XRD and EDAX as shown in Fig. 1. Fig. 1a displays the XRD patterns of the LTO/Ni composite and pristine Li_2TiO_3. The XRD spectrum of LTO/Ni composite exhibits reflection lines (002), (110), ($\bar{1}$31), ($\bar{1}$33), ($\bar{2}$04), (006), (312) and (062), which are characteristic peaks of the monoclinic Li_2TiO_3 phase with $C2/c$ space group (JCPDF cards No. 33-0831). In addition, two distinct reflections at $2\theta = 30.02^o$ and 44.53^o are characteristics of Ni (JCPDF card No. 04-0850) [13]. The sharpness of the XRD patterns gives evidence of the well-defined crystallinity of the LTO. No extra diffraction peak was detected, which demonstrates the purity of LTO. The average coherence length deduced from the Scherrer law for both the LTO/Ni composite and the LTO were 39 nm, respectively.

The EDAX spectrum of the LTO/Ni composite is reported in Figs. 1b and 1c. Only the Ti, O and Ni elements are detected. Li cannot be detected by EDAX, because of its low-characteristic radiation [14, 15]. The elemental composition of this composite deduced from the EDAX spectrum consists of 40 at.% of oxygen (O), 35 at.% of titanium (Ti) and 25 at.% of Ni (accuracy of ±0.5%). The EDS spectrum of the LTO powders exhibited Ti and O elements only, as shown in Fig. 2b, giving another evidence of the phase purity of Li_2TiO_3. The elemental composition of this pristine Li_2TiO_3 consists of 74.5 at.% of O and 25.5 at.% of Ti (accuracy of ±0.5%).

Fig. 2 presents the morphological properties of the LTO/Ni composite studied by FESEM and surface topology experiments. The SEM image of LTO/Ni composite, in which the Ni foam forms a 3D-Ni backbone with large open pores of 100–800 μm in diameter is shown in Fig. 2a. Some protuberances are observed on top of the Ni foam. The slurry of LTO is infused into the Ni foam and the pores are filled by LTO. The protuberances at the surface of the Ni framework are well retained on the top, and the 3D architecture is well preserved during the infusion. The liquefied LTO completely impregnated the Ni foam during the synthesis process. The FESEM image of LTO/Ni nanoparticles is reported in Fig. 2b. The surface of the composite is asperously with many protuberances and a thickness of ≈800 μm. However, owing to their obtuse and bulky form, the integrity of the Li_2TiO_3/3D Ni foam composite was preserved, with the protuberances inside the Ni foam.

LTO nanoparticles spread on the top of Ni foam show well dispersed nearly cubic grains with an estimated average grain size of 49 nm, which matches the coherence length deduced from XRD, so that the grains are monodispersed crystallites. Their size distribution estimated from the J-Software [16] is reported in Fig. 2c. The estimated surface roughness of 28 nm (Fig. 2d), is consistent with the size of the LTO particles.

The TEM image of LTO/Ni composite (Fig. 3a) displays cubic particles with size in the range 30–50 nm. Moreover, all electron diffraction rings have bright spots and sharp (Fig. 3b) indicating that the particles are well crystallized with nanometer scale, in agreement with the XRD results. In the HRTEM image of Li_2TiO_3/Ni composite depicted in Fig. 3c, we observe the spacing between lattice fringes being ~0.47 nm matching well with the d-spacing of the high intense (002) plane of the LTO crystal lattice.

3.2. Li_2TiO_3/Ni foam composite as anode

All the electrochemical tests were conducted at room temperature (25 °C) in three-electrode aqueous cell (Fig. 4). Fig. 4a shows the cyclic voltammetry (CV) curves recorded at 1 mV s^{-1} in the potential range of 0.0–1.0 V. A pair of reduction/oxidation peaks is observed for LTO/Ni foam composite and pristine LTO, which corresponds to the process of insertion and deinsertion of Li$^+$ ions into/from the monoclinic LTO network. The cathodic (reduction) peaks of LTO/Ni composite and
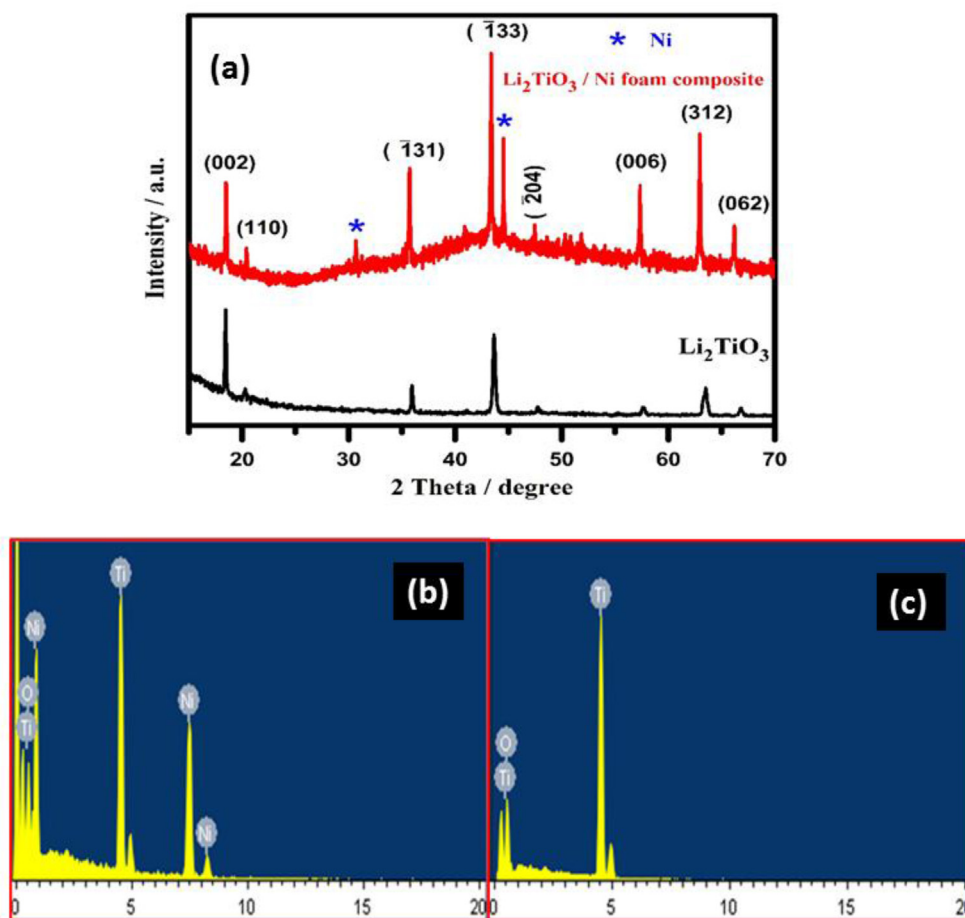
Fig. 1. (a) X-ray diffraction spectra of Li₂TiO₃/Ni foam composite and pristine Li₂TiO₃. (b) Energy-dispersive X-ray spectroscopy (EDAX) spectrum of Li₂TiO₃/Ni foam composite and (c) EDAX spectrum of pristine Li₂TiO₃.

pristine LTO located at 0.304/0.230 V are attributed to the insertion of Li⁺ ions into the active network to form $Li_{2+x}TiO_3$ with $x \approx 0.5$. During reduction, Li⁺ ions are sequentially inserted in empty site of the LiTi₂ interlayers and in plane Li(1), Li(2) sites and create Ti⁺⁴ and O⁻² site vacancies concomitantly with a charge compensation of Ti⁺⁴/Ti⁺³ [17]. It is a reversible process for charging with a charge compensation of Ti⁺³/Ti⁺⁴ for both electrodes. The oxidation (Ti³⁺ to Ti⁴⁺) peaks are originated at 0.703/0.769 V signifies de-intercalation of Li⁺ ions from host structure of LTO/Ni composite and pristine LTO. The polarization value, d*V*, for the redox peaks are 0.304 mV and 0.539 mV for LTO/Ni composite and pristine LTO, respectively. Smaller d*V* for LTO/Ni composite electrode indicates that kinetics of Li⁺ ions faster than in pristine LTO [18, 19, 20]. The Ni foam not only provides high conductivity but also allow for large volume expansion of active materials. In the present work Li₂TiO₃/Ni composite and pristine Li₂TiO₃ do not change their phases during electrochemical process. This is evidenced by the charge-discharge reactions of both electrodes occurring between 0.6-0.7 V (in the battery case shown in Fig. 4b), meaning monoclinic – monoclinic phase transition, and the material is 'zero strain' in the process. The absence of voltage plateau confirms the "non-stoichiometric" behavior of the lithiated compound. Therefore, Li₂TiO₃ shows a good structural stability. The drawback is its low intrinsic conductivity (10⁻¹¹ S cm⁻¹) resulting in low capacity and low rate capability.

The chemical lithium diffusion coefficients, D_{Li}, were calculated using the Randles–Sevick relation (Eq. 1) [21, 22]:

$$i_p = kn^{3/2}AC_0D_{Li}^{1/2}\nu^{1/2}, \tag{1}$$

where i_p is the anodic peak currents from CV plots (0.9569 and 0.176 mA

for LTO/Ni foam composite and pristine LTO, respectively), $k = 2.69 \times 10^5$ is a constant expressed in C mol⁻¹ V⁻¹/², A is the surface area of the anode (1 cm²), n is the number of electrons for Li⁺ transferred, C_o is the concentration of Li ions (2.15×10^{-1} mol L⁻¹), D_{Li+} is the chemical diffusion coefficient of Li, and ν is the scan rate (1 mV s⁻¹). The D_{Li+} value deduced from Eq. (1) for the LTO/Ni composite is 1.12×10^{-10} cm² s⁻¹, which is much higher than that of pristine LTO ($D_{Li+} = 3.81 \times 10^{-11}$ cm² s⁻¹). The vertically aligned scaffold channels of the Ni foam provide robust mechanical adhesion and excellent electrical contact with LTO material and make it possible to expose almost the entire surface, providing many electro-active sites for redox reactions [23]. For pristine LTO, the low electronic conductivity of β-LTO phase is responsible for the slow kinetics of Li⁺-ions with higher polarization value (d*V* = 0.539 mV). Furthermore, the discharged phases were not distorted during cathodic/anodic cycles for LTO electrodes, in agreement with previous report [11].

The charge-discharge curves of the LTO/Ni composite and pristine LTO cycled within the potential range from 0.0 to 1.0 V at 1C rate are shown in Fig. 4b. The discharge curves of LTO/Ni composite and pristine LTO exhibit a S-shape voltage profile at a current density of 1 mA g⁻¹ and corroborates to the Ti⁴⁺/Ti³⁺ reduction [24, 25, 26]. It is assumed that the lithium intercalation-deintercalation can be described by the reaction (Eq. 2):

$$Li_2TiO_3 + xLi^+ + xe^- \leftrightarrows Li_{2+x}TiO_3. \tag{2}$$
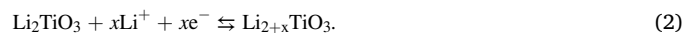
However, according Eq. (2), the LTO/Ni composite delivers a larger initial specific discharge capacity of 153 mAh g⁻¹, against 122 mAh g⁻¹ with a transfer of ~0.5 mol of electrons for pristine LTO. Here, two
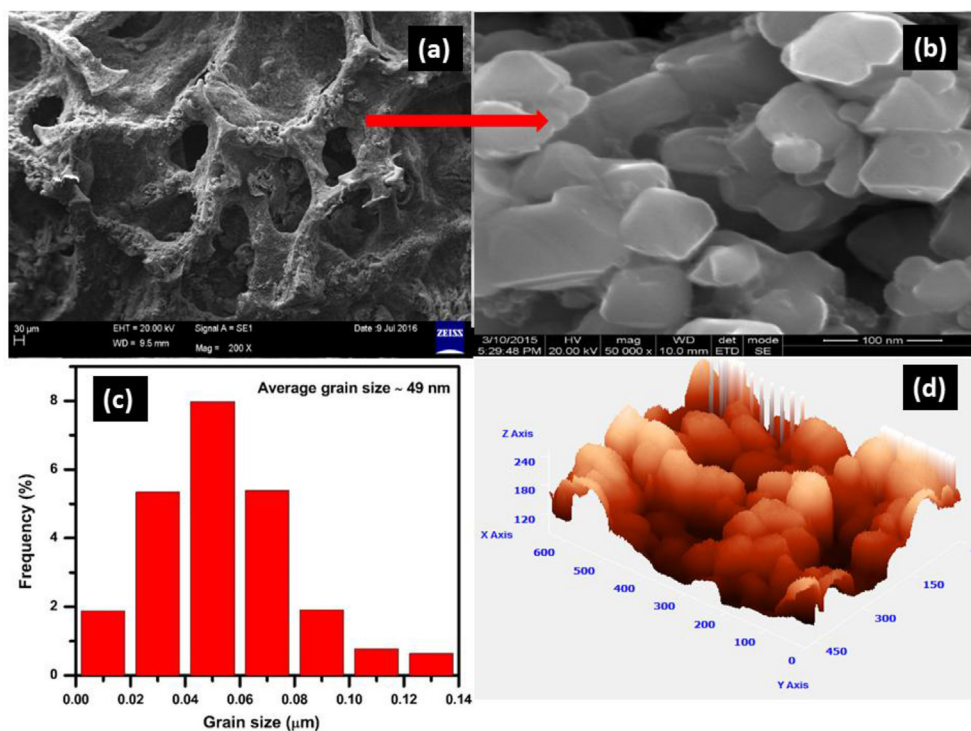
Fig. 2. (a) SEM image of Li$_2$TiO$_3$/Ni foam composite, (b) FESEM image of Li$_2$TiO$_3$ nano particles on Ni foam, (c) Particle size distribution determined from FESEM image and (d) 3D-surface topography of Li$_2$TiO$_3$ nanoparticles. This image was treated via the "image NOVA" software, which generated the z-axis from FESEM data. Numbers are in nm.
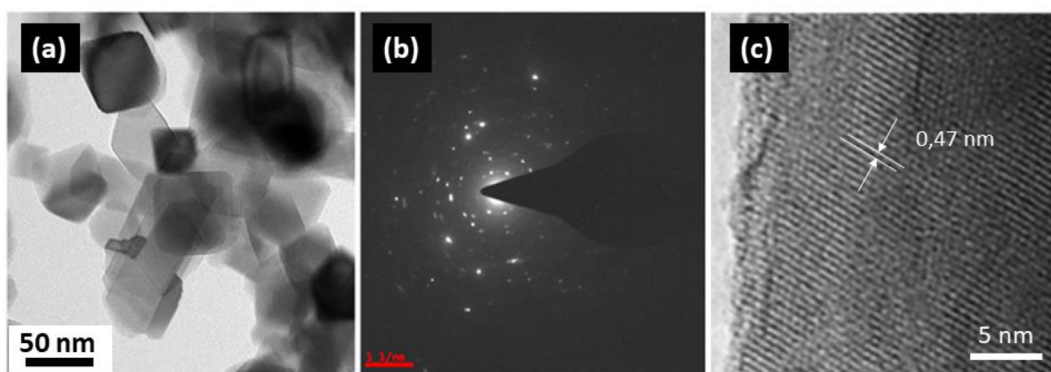
Fig. 3. (a) TEM image of Li$_2$TiO$_3$/Ni foam composite nanoparticles (b) SAED pattern of Li$_2$TiO$_3$/Ni foam composite, (c) HRTEM image of LTO particle of Li$_2$TiO$_3$/Ni foam composite.

reasons can be invoked. First, the well-defined Ni foam with 3D-porous channels falicitates high conductivity to LTO particles and allows an easy access to the electrolyte, which shortens the transfer pathways of ions with enhanced ionic kinetics. Second, the synergistic effects of the two metal ions (Ti and Ni) in the composite provide richer redox chemistry than the individual components [27, 28].

The electrochemical impedance spectra of the Li$_2$TiO$_3$/Ni composite and pristine LTO electrodes were measured in the frequency range from 1 Hz to 1 MHz. The resulting Nyquist plots are shown in Fig. 4c. Each Nyquist curve is composed by a depressed semicircle in the high-frequency region, which is due to the charge transfer resistance (R_{ct}) at the solid-electrolyte interface, and a sloped line in the low-frequency range, which originates from the lithium diffusion-controlled process, i.e. Warburg-type diffusion [29, 30]. The intercept of the impedance on the Z'-real axis in the high frequency region indicates the ohmic resistance (R_s) of the electrodes and electrolyte. The estimated impedance of the pristine LTO electrode is ~250 Ω, and the electrode with Ni foam as

the current collector is ~160 Ω. This suggests that the charge transfer resistance with LTO/Ni composite is much lower that of pristine LTO, due to the good electrical connectivity of the 3D structure. These results reveal that the 3D scaffold network Ni foam not only improves the lithium ion diffusion, but also efficiently enhances the electronic conductivity of the LTO/Ni composite. Fig. 4d displays the specific discharge capacity vs. cycle number of LTO/Ni composite and pristine LTO electrodes over 30 discharge cycles in the voltage region of 0.0–1.0 V at 1C rate. The LTO/Ni composite electrode retained discharge capacity of 145 mAh g^{-1} even after 30 cycles, which is about 95% of its initial capacity. For comparison, the pristine LTO anode retained discharge capacity of 115 mAh g^{-1} even after 30 cycles. The LTO/Ni composite is thus a candidate for energy storage applications [31].

3.3. Li$_2$TiO$_3$/Ni foam as electrode of pseudo-capacitor

The electrochemical properties displayed in the previous section
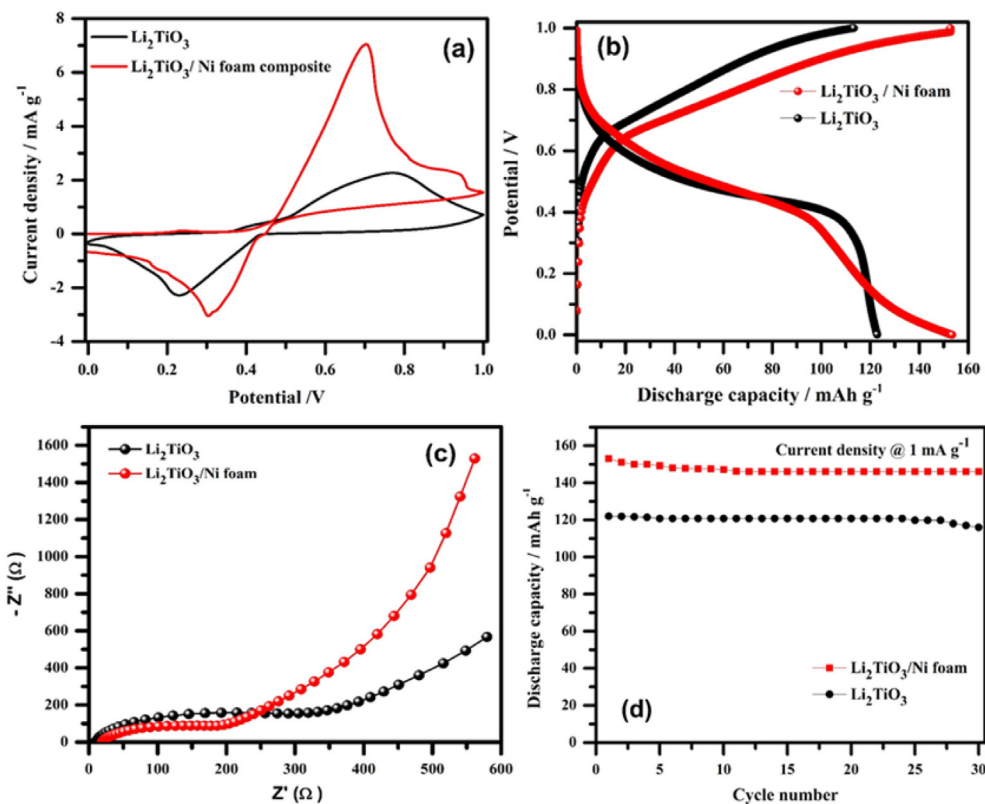
Fig. 4. (a) Cyclic voltammograms of Li$_2$TiO$_3$/Ni foam composite and pristine Li$_2$TiO$_3$ in electrochemical cell. (b) Galvanostatic charge–discharge curves of Li$_2$TiO$_3$/Ni foam composite and pristine Li$_2$TiO$_3$ in electrochemical cell. (c) Electrochemical impedance spectroscopy (EIS) of Li$_2$TiO$_3$/Ni foam composite and pristine Li$_2$TiO$_3$ in electrochemical cell. (d) Cycling performance of Li$_2$TiO$_3$/Ni foam composite and pristine Li$_2$TiO$_3$ in electrochemical cell.
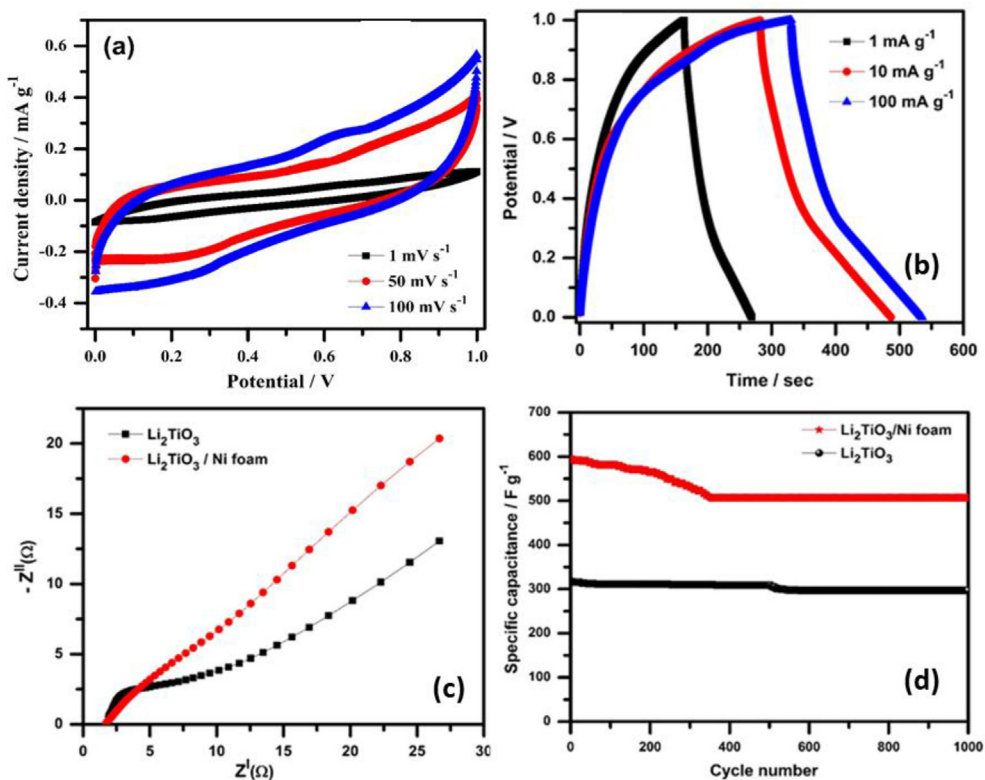
Fig. 5. (a) Cyclic voltammograms of Li$_2$TiO$_3$/Ni foam composite negatrode. (b) Charge-discharge curves Li$_2$TiO$_3$/Ni foam composite negatrode in asymmetric capacitor. (c) Nyquist plots of Li$_2$TiO$_3$/Ni foam composite negatrode and pristine Li$_2$TiO$_3$ negatrode in asymmetric capacitor. (d) Cycling performance of Li$_2$TiO$_3$/Ni foam composite negatrode and pristine Li$_2$TiO$_3$ negatrode in asymmetric capacitor.

suggest that the LTO/Ni composite can be used as a pseudo-capacitor electrode, which, by definition, stores charge via faradic process and involves the transfer of charge between electrode and electrolyte [32]. The pseudocapacitive properties of LTO/Ni electrodes for asymmetric supercapacitor were also tested individually in three-electrode aqueous cell at 25 °C; see Ref. [11] for a comparison with electrochemical properties of pristine LTO electrode of pseudo-capacitor. The electrochemical signatures of the pristine LTO show almost rectangular shape of CV curves at different scan rates from 1-100 mV s^{-1}. The nearly rectangular shaped mirror image CV curves appeared without reduction/oxidation peaks at different currents within the potential range -0.4 to +0.4 V, which demonstrates that the electrochemical process occurs with both faradic reaction and double-layer capacitance, i.e. the capacitive behavior of pristine LTO negatrode. It was evidenced that the area of CV curves for pristine LTO is increased by increasing scan rates from 1 to 100 mV s^{-1} showing a good rate capability of the electrode in asymmetric supercapacitors [11]. The CV of LTO/Ni composite electrode at various scan rates (i.e., 1, 50, 100 mV s^{-1}) within the potential range 0.0 to +1.0 V is shown in Fig. 5a. For the LTO/Ni composite electrode, the CV curves demonstrate the quasi rectangular CV profiles that simply pseudo-capacitive behavior. The CV curves show broad shape at reduction and oxidation peaks associated to the faradic reaction. Note that such a behavior was also observed for Ni(OH)$_2$ and V$_2$O$_5$/polyaniline layer-by-layer electrodes [33, 34, 35]. Furthermore, the area of CV curves for LTO/Ni composite is enhanced by increasing the scan rates from 1 to 100 mV s^{-1}, which represents a good rate capability. It can be observed that the CV profile of LTO/Ni foam composite demonstrate high integral area with high currents at different scan rates while comparing to pristine LTO indicating that the 3D scaffold Ni foam plays a significant role to improve the conductivity and provide high surface to redox reactions [37].

Fig. 5b displays the charge–discharge curves of LTO/Ni composite as asymmetric supercapacitor electrode at current density of 1, 10 and 100 mA g^{-1} in the potential range 0.0 to +1.0 V. The nonlinear shape charge and discharge curves at various current densities indicate a pseudocapacitive behavior. The discharge curve of LTO/Ni composite is composed of three regions: a small drop of voltage due to the internal resistance, a linear deviation of the time dependent potential (double-layer capacitance behavior), and slight slope variation of the time dependence of the charge transfer reaction of LTO/Ni composite corroborating the CV profile [38]. The specific capacitance can be estimated by the relation (Eq. 3):

$$C_{sp} = \frac{I}{m} \frac{dt}{dV},\qquad(3)$$

where C_{sp} is the specific capacitance (in F g^{-1}), I is the charge/discharge current, t is the time of discharge, V is the voltage difference between the upper and lower potential limits, and m is the mass of the active material [39]. Using Eq. (3), the specific capacitance of the LTO/Ni composite was found to be 593, 502 and 450 F g^{-1} at current densities of 1, 10 and 100 mA g^{-1}, respectively. The change in potential window of LTO/Ni composite is attributed to the lower particle size and Ni foam skeleton. The scaffold Ni foam plays a significant role to improve conductivity among the LTO particles and improve also kinetics of the reaction preserving the same potential window in the case of LTO/Ni composite [37]. These results can be compared with data from pristine LTO asymmetric supercapacitor with specific capacitances of 317, 198, 165, 141, 120 and 111 F g^{-1} are obtained at current densities of 1, 2, 5, 10, 50 and 100 mA g^{-1}, respectively [11]. Nickel foam has been selected by several workers as a cost-effective substrate investigating active materials (AM) prepared by a slurry with low amount of carbon black (≤15 wt.%) [40, 41, 42, 43]. Aziz et al. studied the pseudocapacitive properties of Na$_2$Ti$_2$O$_4$(OH)$_2$ using a AM:AC:PVDF (85:5:10) electrode [40]. Ali et al. investigated an electrode made by mix up the 80:15:5 slurry deposited on Ni foam [41]. The electrode prepared by Li et al. had an 8:1:1 mass ratio [42]. Guan

et al. reported the high specific capacitance of the hybrid structure of cobalt monoxide nanowire@nickel hydroxidenitrate nanoflake aligned on nickel foam as a result of a synergic effect of both active materials as well as the nickel foam [43]. A nickel foam tested independently shows a capacitance of only 2 F g^{-1} at a current density of 5 mA cm^2 that is only 2.89% of the total capacitance of the hybrid structure. To verify the optimum composition of the electrode slurry, we test the capacitance of Li$_2$TiO$_3$ by increasing the amount of carbon black to be comparable to the mass of Ni foam. Results are listed in Table 1. Larger amounts of carbon only decrease the capacitance. The carbon black pressed onto Ni foam shows only a capacitance of ~100 F g^{-1}. We found the best specific capacitance of 317 F g^{-1} at 80:10:10 for pristine Li$_2$TiO$_3$. The same composition has been employed for Li$_2$TiO$_3$/Ni foam composite electrode preparation and observed enhanced specific capacitance of 593 F g^{-1}, since Ni foam provides high conductive network. Note that the nickel foam is the current collector, and as such, is excluded from the calculation of the specific capacitance as usual.

The electrochemical behavior of LTO/Ni foam composite negatrode was further studied by EIS. Fig. 5c shows the Nyquist plots of the LTO/Ni foam composite and pristine LTO electrodes recorded in the frequency range from 1 Hz to 1 MHz, with an ac excitation signal of 5 mV. The LTO/Ni composite displays a smaller resistance value, i.e. $R_s = 4\ \Omega$ and $R_{ct} = 2\ \Omega$, against $R_s = 4\ \Omega$, and $R_{ct} = 8\ \Omega$ for pristine LTO. Moreover, the LTO/Ni composite exhibits a nearly straight line that is closer to vertical line in the low-frequency region, indicating a good capacitive behavior of the electrode in the Li$_2$SO$_4$ aqueous solution in agreement with the results of the electrochemical measurements. The cycling performance of the electrode is shown in Fig. 5d. The LTO/Ni composite electrode exhibited stable electrochemical behavior, with a capacitance of 563 F g^{-1} after 1,000 cycles at a current density of 1 mA g^{-1}, which amounts to a capacitance retention of 95%, whereas pristine LTO retained 92% capacitance after 1,000 cycles. Note that a sudden voltage drop and conspicuous voltage fluctuation were detected after 400 cycles, which was attributed to unstable property of intrinsic solid electrolyte interface (SEI) on Li-metal based electrodes faced the initial cycles [44, 45, 46].

With respect to electrical double-layer capacitors, pseudo-capacitors have a higher specific capacitance and higher energy density, which justifies the interest in these materials. However, they also suffer from a reduced cycling life and smaller power density, because they process via an oxidation-reduction reaction just like batteries [47, 48]. Therefore, our results should be discussed with respect to other electrode materials for pseudo-capacitors only. In this context, materials used in electrodes fabrication are metal oxides. They have been reviewed for instance in Ref. [49]. The archetype is RuO$_2$ [50], prepared by electrodeposition, yielding a specific capacitance of 498 F g^{-1} at a scan rate of 5 mV s^{-1} [51]. A capacitance of 1580 F g^{-1} [52] was obtained with a composite of activated carbon mixed with sol-gel derived RuO$_x$•nH$_2$O nanodots coated on graphite. A nanotubular array of RuO$_x$•nH$_2$O synthesized by template method exhibited a capacitance of 1300 F g^{-1} [53] confirming the superior capacitance obtained with hydrides. However, ruthenium is rare and very expensive, and the typical metal oxide used as electrode for pseudocapacitors is MnO$_2$, which has focused attention owing to its much lower cost compared to RuO$_2$. The three-dimensional MnO$_2$ electrode material showed a specific capacitance of 200 F g^{-1} [54]. 2D nanosheets of MnO$_2$ prepared by exfoliation-reassembling method showed a capacitance of 140–160 F g^{-1} with a cycling stability of ~93–99% up to 1000 cycles [55], while 250 F g^{-1} was obtained with amorphous nanostructured MnO$_2$ synthesized by the mixing of KMnO$_4$ with ethylene glycol [56]. Better results with MnO$_2$ were obtained only in composites with conductive carbon and/or conductive polymer. In particular a capacitance of 281 F g^{-1} was obtained with CNT/polypyrrole/MnO$_2$ [57]. A capacitance of 310 F g^{-1} at 2 mV s^{-1} was obtained with nano-MnO$_2$ on graphene [58]. Other carbon-based manganese oxide composites used as pseudo-capacitor electrodes include carbon/-α-MnO$_2$ (235 F g^{-1}) [59], MnO$_2$/CNTs (374 F g^{-1}) [60]. A smaller capacitance of 234 F g^{-1} was reported for MnO$_2$ loaded on porous

Table 1

Specific capacitance of electrodes with various compositions of LTO:CB:PVDF deposited on Ni foam (4 mg). Result from the CB/Ni electrode is also represented for comparison.

Electrode composition	Mass ratio C/Ni	Specific capacitance (F g^{-1})
80:10:10	9%	593
70:20:10	18%	548
60:30:10	27%	455
50:40:10	36%	392
40:60:10	54%	236
CB	100%	~100

graphene gel/Ni foam, but the cycling stability was remarkable, with less than 1.5% decay after 10 000 cycles [61]. The best capacitance was reported with MnO_2/PPy thin film electrodes electrochemically synthesized over polished graphite substrates, with a capacitance of 620 F g^{-1} [62]. In this case, MnO_2 nanoparticles were embedded within the porous polypyrrole matrix. This result out performs the pseudo-capacitance reported for other MnO_2/PPy composites (see [63, 64] and references therein) even if in all cases the capacitance is found larger than the separate contributions of MnO_2 and PPy, so that the synthesis process is important to optimize the MnO_2-PPy interaction. Nevertheless, the pseudo-capacitive properties in Ref. [62] give evidence of the remarkable performance of this conductive polymer as a host for metal oxides, already known for its performance when it is associated to graphene nanosheets [65]. The capacitance we have obtained with LTO/Ni foam composite is larger than the capacitance reported for any MnO_2-based pseudo-capacitor except MnO_2/PPy. On one hand, this result suggests that LTO can be effectively used as a performing supercapacitor element. On another hand, it is also a motivation for further works and in particular the investigation of LTO/PPy composites.

4. Conclusions

The nanocrystalline LTO and LTO/Ni foam composites were prepared by employing solid state reaction method. The XRD spectrum of LTO/Ni composite exhibited the similar orientations with pristine LTO. The electrochemical properties of LTO/Ni composites are tested in 3–electrode aqueous cell with cut off voltage 0.0–1.0 V. The charge–discharge curves exhibited an initial discharge capacity of 153 mAh g^{-1} at a current density of 1 mA g^{-1} and retained discharge capacity of 95% even after 30 cycles. On the other hand, LTO/Ni composite also exhibited quasi rectangular shaped cyclic voltammetry curves at 1 mV s^{-1} scan rate, characteristic of pseudo-capacitive behavior. The composite delivered a specific capacitance of 593 F g^{-1} at a current density of 1 mA g^{-1} and retained 95 % capacity even after 1000 cycles. Whether it is considered as an anode for Li-ion batteries or as an element of supercapacitance, the 3D scaffold Ni foam plays significant role to improve the conductivity among the LTO nanoparticles. The LTO/Ni composite electrode can thus be considered as a promising electrode for energy storage devices.

Declarations

Author contribution statement

Ambadi Lakshmi-Narayana, Merum Dhananjaya, Nunna Guru-Prakash: Performed the experiments; Analyzed and interpreted the data; Contributed reagents, materials, analysis tools or data.

Alain Mauger: Analyzed and interpreted the data; Critically revising the paper content.

Christian M. Julien: Conceived the experiments; Analyzed and interpreted the data; Wrote the paper.

Obili M Hussain: Conceived and designed the experiments; Analyzed and interpreted the data.

Competing interest statement

The authors declare no conflict of interest.

Additional information

No additional information is available for this paper

References

[1] L. Liu, Z. Hu, L. Sun, G. Gao, X. Liu, Controlled synthesis and enhanced electrochemical performance of Prussian blue analogue-derived hollow $FeCo_2O_4$ nanospheres as lithium-ion battery anodes, RSC Adv. 5 (2015) 36575–36581.

[2] C. Yuan, H.B. Wu, Y. Xie, X.W. Lou, Mixed transition-metal oxides: design, synthesis, and energy-related applications, Angew. Chem. Int. Ed. 53 (2014) 1488–1504.

[3] W. Wang, M. Tian, A. Abdulagatov, S.M. George, Y.C. Lee, R. Yang, Three-dimensional Ni/TiO_2 nanowire network for high areal capacity lithium ion microbattery applications, Nano Lett. 12 (2012) 655–660.

[4] X. Wang, S. Ni, G. Zhou, X. Sun, F. Yang, J. Wang, D. He, Facile synthesis of ultra-long α-MnO_2 nanowires and their microwave absorption properties, Mater. Lett. 64 (2010) 1496–1498.

[5] C.-H. Jung, S.J. Lee, W.M. Kriven, J.-Y. Park, W.-S. Ryu, A polymer solution technique for the synthesis of nano-sized Li_2TiO_3 ceramic breeder powders, J. Nucl. Mater. 373 (2008) 194–198.

[6] Y. Gu, F. Jian, X. Wang, Synthesis and characterization of nanostructured Co_3O_4 fibers used as anode materials for lithium ion batteries, Thin Solid Films 517 (2008) 652–655.

[7] K.T. Nam, D.W. Kim, P.J. Yoo, C.Y. Chiang, N. Meethong, P.T. Hammond, Y.M. Chiang, A.M. Belcher, Virus-enabled synthesis and assembly of nanowires for lithium ion battery electrodes, Science 312 (2006) 885–888.

[8] X.W. Lou, D. Deng, J.Y. Lee, J. Feng, L.A. Archer, Self-supported formation of needlelike Co_3O_4 nanotubes and their application as lithium-ion battery electrodes, Adv. Mater. 20 (2008) 258.

[9] Y. Shi, B. Guo, S.A. Corr, Q. Shi, Y.S. Hu, K.R. Heier, L. Chen, R. Seshadri, G.D. Stucky, Ordered mesoporous metallic MoO_2 materials with highly reversible lithium storage capacity, Nano Lett. 9 (2009) 4215–4220.

[10] Q. Sa, Y. Wang, Ni foam as the current collector for high capacity C–Si composite electrode, J. Power Sources 208 (2012) 46–51.

[11] A. Lakshmi-Narayana, M. Dhananjaya, N. Guru-Prakash, O.M. Hussain, C.M. Julien, Nanocrystalline Li_2TiO_3 electrodes for supercapattery application, Ionics 23 (2017) 3419–3428.

[12] A. Eftekhari, Low voltage anode materials for lithium-ion batteries, Energy Storage Mater. 7 (2017) 157–180.

[13] L.A. García-Cerda, K.M. Bernal-Ramos, Sagrario M. Montemayor, M.A. Quevedo-López, R. Betancourt-Galindo, D. Bueno-Báques, Preparation of hcp and fcc Ni and Ni/NiO nanoparticles using a citric acid assisted Pechini-type method, J. Nanomater 2011 (2011), 162495.

[14] P. Rosaiah, O.M. Hussain, Synthesis, electrical and dielectric properties of lithium iron oxide, Adv. Mater. Lett. 4 (2013) 288–295.

[15] Y. Kojima, K. Suzuki, Y. Kawai, Hydrogen generation from lithium borohydride solution over nano-sized platinum dispersed on $LiCoO_2$, J. Power Sources 155 (2006) 325–328.

[16] N. Rishi, Rana, Particle size and shape analysis using images with customized tools for segmentation of particles, Int. J. Eng. Res. Technol. 11 (2015), 2778-0181.

[17] Y.Z. Hao, Q.L. Zhang, J. Zhang, C.R. Xin, H. Yang, Enhanced sintering characteristics and microwave dielectric properties of Li_2TiO_3 due to nano-size and nonstoichiometry effect, J. Mater. Chem. 22 (2012) 23885–23892.

[18] K.M. Colbow, J.R. Dahn, R.R. Haering, Structure and electrochemistry of the spinel oxides $LiTi_2O_4$ and $Li_{43}Ti_{53}O_4$, J. Power Sources 26 (1989) 397–402.

[19] P. Krtil, D. Fattakhova, Li insertion into Li-Ti-O spinels: voltammetric and electrochemical impedance spectroscopy study, J. Electrochem. Soc. 148 (2011) A1045–A1050.

[20] J. Shu, Li–Ti–O compounds and carbon-coated Li–Ti–O compounds as anode materials for lithium ion batteries, Electrochim. Acta 54 (2009) 2869–2876.

[21] C.M. Julien, A. Mauger, H. Groult, K. Zaghib, Surface modification of positive electrode materials for lithium-ion batteries, Thin Solid Films 572 (2014) 200–207.

[22] K. Sivajee-Ganesh, B. Purusottam-Reddy, P. Jeevan-Kumar, K. Jayanthbabu, P. Rosaiah, O.M. Hussain, Microstructural and electrochemical properties of $LiTi_yCo_{1-y}O_2$ film cathodes prepared by RF sputtering, J. Solid State Electrochem. 19 (2015) 3621–3627.

[23] S. Min, C. Zhao, Z. Zhang, G. Chen, X. Qian, Z. Guo, Synthesis of Ni(OH)$_2$/RGO pseudocomposite on nickel foam for supercapacitors with superior performance, J. Mater. Chem. 3 (2015) 3641–3650.

[24] T. Ohzuku, A. Ueda, N. Yamamoto, Zero strain insertion material of Li[Li$_{1/3}$Ti$_{5/3}$]O$_4$ for rechargeable lithium cells, J. Electrochem. Soc. 142 (1995) 1431–1435.

[25] C. Bohnke, J.L. Fourquet, N. Randrianantoandro, T. Brousse, O. Crosnier, Electrochemical insertion of lithium into the ramsdellite-type oxide Li$_2$Ti$_3$O$_7$: influence of the Li$_2$Ti$_3$O$_7$ particle size, J. Solid State Electrochem. 6 (2002) 403–411.

[26] M.E. Arroyo y de Dompablo, A. Varez, F.G. Alvarado, Structural study of electrochemically obtained Li$_{2+x}$Ti$_3$O$_7$, J. Solid State Chem. 153 (2000) 132–139.

[27] S. Min, C. Zhao, P. Ju, T. Zhou, H. Gao, Y. Zheng, H. Wang, G. Chen, X. Qian, Z. Guo, Facile synthesis of nickel-foam-based nano-architectural composites as binder-free anodes for high capacity Li-ion batteries, J. Power Sources 304 (2016) 311–318.

[28] S.S. Chi, Y. Liu, W.L. Song, L.Z. Fan, Q. Zhang, Prestoring lithium into stable 3D nickel foam host as dendrite-free lithium metal anode, Adv. Funct. Mater. 27 (2017) 1700348–1700358.

[29] C.H. Gao, H.L. Zhao, P.P. Lv, T.H. Zhang, Q. Xia, J. Wang, Engineered Si sandwich electrode: Si nanoparticles/graphite sheet hybrid on Ni foam for next-generation high-performance lithium-ion batteries, ACS Appl. Mater. Interfaces 7 (2015) 1693–1698.

[30] Y.C. Dong, Z.Y. Zhang, Y. Xia, Y.S. Chui, J.M. Lee, J.A. Zapien, Green and facile synthesis of Fe$_3$O$_4$ and graphene nanocomposites with enhanced rate capability and cycling stability for lithium ion batteries, J. Mater. Chem. 3 (2015) 16206–16212.

[31] L. Liu, H. Zhang, Y. Mu, J. Yang, Y. Wang, Porous iron cobaltate nanoneedles array on nickel foam as anode materials for lithium-ion batteries with enhanced electrochemical performance, ACS Appl. Mater. Interfaces 8 (2016) 1351–1359.

[32] S. Mohapatra, A. Acharya, G.S. Roy, The role of nanomaterials for the design of supercapacitors, Lat. Am. J. Phys. Educ. 6 (2012) 380–384.

[33] J. Liu, C. Cheng, W. Zhou, H. Li, H.J. Fan, Ultrathin nickel hydroxidenitrate nanoflakes branched on nanowire arrays for high-rate pseudocapacitive energy storage, Chem. Commun. 47 (2011) 3436–3438.

[34] A.J. Bard, L.R. Faulkner, Electrochemical Methods: Fundamentals and Applications, Wiley & Sons, Inc., New York, 2001, p. 226.

[35] T. Brousse, D. Bélanger, J.W. Long, To be or not to be pseudocapacitive? J. Electrochem. Soc. 162 (2015) A5185–A5189.

[37] H.K. Kang, S.G. Woo, J.H. Kim, S.R. Lee, Y.J. Kim, Conductive porous carbon film as a lithium metal storage medium, Electrochim. Acta 176 (2015) 172–178.

[38] Y.C. Tsai, W.D. Yang, K.C. Lee, C.M. Huang, An effective electrodeposition mode for porous MnO$_2$/Ni foam composite for asymmetric supercapacitors, Materials 9 (2016) 246–258.

[39] B. Purusottam-Reddy, K. Sivajee-Ganesh, K. Jayanth-Babu, O.M. Hussain, C.M. Julien, Microstructure and supercapacitive properties of rf-sputtered copper oxide thin films: influence of O$_2$/Ar ratio, Ionics 21 (2015) 2319–2328.

[40] R.A. Aziz, I.I. Misnon, K.F. Chong, M.M. Yusoff, R. Jose, Layered sodium titanate nanostructures as a new electrode for high energy density supercapacitors, Electrochim. Acta 113 (2013) 141–148.

[41] G.A.M. Ali, O.A.G. Wahba, A./M. Hassan, O.A. Fouad, K.F. Chong, Calcium-based nanosized mixed metal oxides for supercapacitor application, Ceram. Intern. 41 (2015) 8230–8234.

[42] Y. Li, L. Cao, L. Qiao, M. Zhou, Y. Yang, P. Xiao, Y. Zhang, Ni-Co sulfides nanowires on nickel foam with ultrahigh capacitance for asymmetric supercapacitor, J. Mater. Chem. 2 (2014) 6540–6548.

[43] C. Guan, J. Liu, C. Cheng, H. Li, X. Li, W. Zhou, H. Zhang, H.J. Fan, Hybrid structure of cobalt monoxide nanowire@nickel hydroxidenitrate nanoflake aligned on nickel foam for high-rate supercapacitor, Energy Environ. Sci. 4 (2011) 4496–4499.

[44] Y. Lu, Z. Tu, L.A. Archer, Stable lithium electrodeposition in liquid and nanoporous solid electrolytes, Nat. Mater. 13 (2014) 961–969.

[45] Z. Liang, D.C. Lin, J. Zhao, Z.D. Lu, Y.Y. Liu, C. Liu, Y.Y. Lu, H.T. Wang, K. Yan, X.Y. Tao, Y. Cui, Composite lithium metal anode by melt infusion of lithium into a 3D scaffold with lithiophilic coating, Proc. Natl. Acad. Sci. U.S.A. 113 (2016) 2862–2867.

[46] G. Bieker, M. Winter, P. Bieker, Electrochemical in situ investigations of SEI and dendrite formation on the lithium metal anode, Phys. Chem. Chem. Phys. 17 (2015) 8670–8679.

[47] S.M. Chen, R. Ramachandran, V. Mani, R. Saraswathi, Recent advancements in electrode materials for the high performance electrochemical supercapacitors: a review, Int. J. Electrochem. Sci. 9 (2014) 4072–4085.

[48] T. Chen, L. Dai, Carbon nanomaterials for high-performance supercapacitors, Mater. Today 16 (2013) 272–280.

[49] Z.S. Iro, C. Subramani, S.S. Dash, A brief review on electrode materials for supercapacitor, Int. J. Electrochem. Sci. 11 (2016) 10628–10643.

[50] C. Zhao, W. Zheng, A review for aqueous electrochemical supercapacitors, Frontiers Energy Res (2015) 1–11.

[51] T.P. Gujar, W.Y. Kim, I. Puspitasari, K.D. Jung, O.S. Joo, Electrochemically deposited nanograin ruthenium oxide as a pseudocapacitive electrode, Int. J. Electrochem. Sci. 2 (2007) 666–673.

[52] C.C. Hu, W.C. Chen, K.H. Chang, How to achieve maximum utilization of hydrous ruthenium oxide for supercapacitors, J. Electrochem. Soc. 151 (2004) A281–A290.

[53] C.C. Hu, K.S. Chang, M.C. Lin, Y.T. Wu, Design and tailoring of the nanotubular arrayed architecture of hydrous RuO$_2$ for next generation supercapacitors, Nano Lett. 6 (2006) 2690–2695.

[54] Y.T. Wang, A.H. Lu, H.L. Zhang, W.C. Li, Synthesis of nanostructured mesoporous manganese oxides with three-dimensional frameworks and their application in supercapacitors, J. Phys. Chem. C 115 (2011) 5413–5421.

[55] M.S. Song, K.M. Lee, Y.R. Lee, I.Y. Kim, T.W. Kim, J.L. Gunjakar, S.J. Hwang, Porously assembled 2D nanosheets of alkali metal manganese oxides with highly reversible pseudocapacitance behaviors, J. Phys. Chem. C 114 (2010) 22134–22140.

[56] P. Regupathy, D.H. Park, G. Campet, H.N. Vasan, S.J. Hwang, J.H. Choy, N. Munichandraiah, Remarkable capacity retention of nanostructured manganese oxide upon cycling as an electrode material for supercapacitor, J. Phys. Chem. C 113 (2009) 6303–6309.

[57] S.R. Sivakkumar, J.M. Ko, D.Y. Kim, B.C. Kim, G.G. Wallace, Performance evaluation of CNT/polypyrrole/MnO$_2$ composite electrodes for electrochemical capacitors, Electrochim. Acta 52 (2007) 7377–7385.

[58] J. Yan, Z. Fan, T. Wei, W. Qian, M. Zhang, F. Wei, Fast and reversible surface redox reaction of graphene–MnO$_2$composites as supercapacitor electrodes, Carbon 48 (2010) 3825–3833.

[59] A.J. Roberts, R.C.T. Slade, Effect of specific surface area on capacitance in asymmetric carbon/α-MnO$_2$ supercapacitors, Electrochim. Acta 55 (2010) 7460–7469.

[60] J.G. Wang, Y. Yang, Z.H. Huang, F. Kang, Synthesis and electrochemical performance of MnO$_2$/CNTs–embedded carbon nanofibers nanocomposites for supercapacitors, Electrochim. Acta 75 (2012) 213–219.

[61] T. Zhai, F.X. Wang, M.H. Yu, S.L. Xie, C.L. Liang, C. Li, F.M. Xiao, R.H. Tang, Q.X. Wu, X.H. Lu, Y.X. Tong, 3D MnO$_2$–graphene composites with large areal capacitance for high-performance asymmetric supercapacitors, Nanoscale 5 (2013) 6790–6796.

[62] R.K. Sharma, A.C. Rastogi, S.B. Desu, Manganese oxide embedded polypyrrole nanocomposites for electrochemical supercapacitor, Electrochim. Acta 53 (2008) 7690–7695.

[63] A. Bahloul, B. Nessark, E. Briot, H. Groult, A. Mauger, K. Zaghib, C.M. Julien, Polypyrrole-covered MnO$_2$ as electrode material for supercapacitor, J. Power Sources 240 (2013) 267–272.

[64] L. Yuan, C. Wan, L. Zhao, Facial in-situ synthesis of MnO$_2$/PPy composite for supercapacitor, Int. J. Electrochem. Sci. 10 (2015) 9456–9465.

[65] S. Biswas, L.T. Drzal, Multilayered nanoarchitecture of graphene nanosheets and polypyrrole nanowires for high performance supercapacitor electrodes, Chem. Mater. 22 (2010) 5667–5671.